Nuclear Instruments and Methods in Physics Research A254 (1987) 26–34
North-Holland, Amsterdam

AN ELECTROMAGNETIC CALORIMETER WITH WAVELENGTH SHIFTING FIBER READOUT

B. LOEHR

Deutsches Elektronen-Synchrotron DESY, Hamburg, FRG

S. WEISSENRIEDER

Universität Hamburg, II.Institut für Experimentalphysik, Hamburg, FRG

F. BARREIRO and E. ROS

Universidad Autónoma de Madrid, Spain

Received 6 August 1986

We investigate the response of an electromagnetic calorimeter using wavelength shifting fibers for the readout. The calorimeter is a sandwich of lead and scintillator plates and the fibers are inserted into holes perpendicular to the plates. We study in particular light yield, uniformity of response and energy resolution. We also present a Monte Carlo interpretation of our experimental results.

1. Introduction

A characteristic of the detectors planned for the electron–proton collider HERA [1], presently under construction at DESY, is the use of large calorimeters. They have to be compact, cover a large solid angle, and present a high granularity in the readout. The energy and angular resolution of the calorimeter determines to a great extent the performance of the whole detector.

As part of the design studies for the ZEUS detector [2] at HERA, we have constructed and tested several electromagnetic calorimeter modules with an optical fiber readout system, in order to investigate the energy resolution, uniformity of the response and photoelectron yield. Other experimental results on the same subject can be found in ref. [3].

2. Description of the modules and experimental setup

Each calorimeter module is a sandwich of 70 lead plates and 70 scintillator plates (see a schematic drawing in fig. 1). The thickness of the lead plates is 2 mm and the thickness of the scintillator plates is 5 mm. The total size of a module is $19 \times 19 \times 49$ cm^3, the total length is 25.8 radiation lengths and the Molière radius about 6 cm.

The light produced in the scintillator is collected by 16 optical fibers connected via a piece of lucite light guide to a photomultiplier placed at the rear of the calorimeter. These fibers are inserted into 16 holes of 2 mm diameter drilled perpendicularly to the plates. We used optical fibers [4] of 1.5 mm diameter containing a wavelength shifting agent. They consist of a polystyrene core (refractive index: 1.59) doped with 400 mg/l of K-27 [5] and a cladding of polymethylmetacrylat (PMMA, refractive index: 1.46). The average fiber length was 120 cm. We used two scintillator materials, KSTI-390 [6] and SCSN-38 [7]. The edges of the plates were polished and the plates themselves wrapped in reflective aluminum foil. The surfaces of the holes in the scintillator were not polished after drilling. The module equipped with the KSTI-390 scintillator will be referred to in the following as module A, and the one equipped

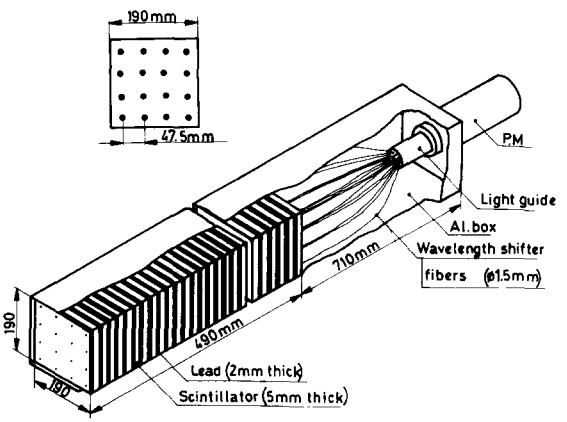

Fig. 1. A schematic view of a calorimeter module.

0168-9002/87/$03.50

Table 1
Description of the modules and summary of the results

	Module A	Module B
Number of fibers	16	16
Diameter of fibers	1.5 mm	1.5 mm
Fiber material	polystyrene	polystyrene
Fiber doping	K27 400 mg/l	K27 400 mg/l
Scintillator	KSTI-390	SCSN-38
Diameter of holes in scintillator	2.5 mm	2.0 mm
Phototube	56DVP	XP2011
$\sigma/\sqrt{E}$ (E in GeV)	$(13.1\pm0.8)\%$ $\oplus(2.2\pm1.4)\%\sqrt{E}$	$(8.6\pm0.3)\%$ $\oplus(1.9\pm0.5)\%\sqrt{E}$
Method for photostatistics	grey filter	LED
$\sigma_{ph}/\sqrt{E}$ (E in GeV)	$(9.0\pm1.0)\%$	$(5.6\pm0.3)\%$
$\sigma_{other}/\sqrt{E}$ (E in GeV)	$(9.5\pm1.5)\%$	$(6.5\pm0.5)\%$
Photoelectrons per MeV	0.7 ± 0.2	1.7 ± 0.2

with SCSN-38 as module B. Module A had a photomultiplier Valvo 56DVP and module B an XP2011. Table 1 summarizes the description of both calorimeters.

These modules were tested in a DESY test beam which provided electrons from 1 to 5 GeV. The momentum spread of this beam was found to be at most 3% from a measurement with a BGO crystal. The modules were installed on a remotely controlled movable support allowing the impact point of the incident beam on the calorimeter to be varied. The trigger was defined with the help of two pairs of crossed scintillation counters defining a beam size of 5×5 mm^2 at the front face of the calorimeter. A veto counter with a central hole of 2 cm diameter was used to reject beam halo particles. The experimental setup in the beamline is shown in fig. 2. The photomultiplier signal was integrated by a LeCroy ADC 2249A with a gate time of 140 ns. The ADC output was read into a NORD computer and transferred to the DESY IBM for off-line analysis.

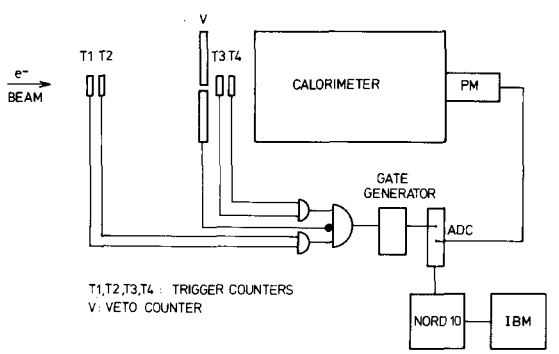

Fig. 2. A schematic view of the experimental setup.

3. Linearity and resolution at the center of the module

We measured the response of the two calorimeter modules to incident electrons of 1 to 5 GeV. The main results are summarized in table 1. The calorimeter response and resolution as a function of the energy for an incident beam at the center of the module are displayed in figs. 3a and b. Both modules show a linear response with deviations less than 1% for energies in the range between 1 and 5 GeV.

The measured resolutions suggest an energy dependence of the type:

$$\frac{\sigma}{E} = \frac{a}{\sqrt{E}} \oplus b$$

($\oplus$ means the square root of a quadratic sum). The fitted values for both calorimeters are (for E in GeV):

$a = (13.1 \pm 0.8)\%$, $b = (2.2 \pm 1.4)\%$ for module A,
$a = (\ 8.6 \pm 0.3)\%$, $b = (1.9 \pm 0.5)\%$ for module B.

The constant term b is compatible with the beam resolution. The parameter a includes mainly the resolution of the calorimeter due to sampling fluctuations and also the fluctuation due to photelectron statistics.

The contribution to the resolution due to fluctuations in the number of photoelectrons released at the cathode of the photomultiplier (σ_{ph} in table 1) has been determined by two different methods. In the first, a grey filter is inserted between the light guide and the photocathode and the pulse height is consequently reduced by a factor f; then σ_{ph} is determined according to the formula:

$$\sigma_{ph} = \sqrt{\frac{\sigma_2^2 - \sigma_1^2}{f-1}},$$

where σ_2 and σ_1 are the resolutions with and without grey filter respectively. In the second method, the pulse height of a light emitting diode (LED), mounted in front of the tube, is tuned to the same value as the calorimeter signal. Under the assumption that the LED delivers a stable light output during the measurement time, the width of the pulse height distribution directly gives σ_{ph}. Both methods were checked against each other, giving compatible results.

The measured resolutions are:

$\sigma_{ph} = (9.0 \pm 1.0)\%\sqrt{E}$ for module A,
$\sigma_{ph} = (5.6 \pm 0.3)\%\sqrt{E}$ for module B.

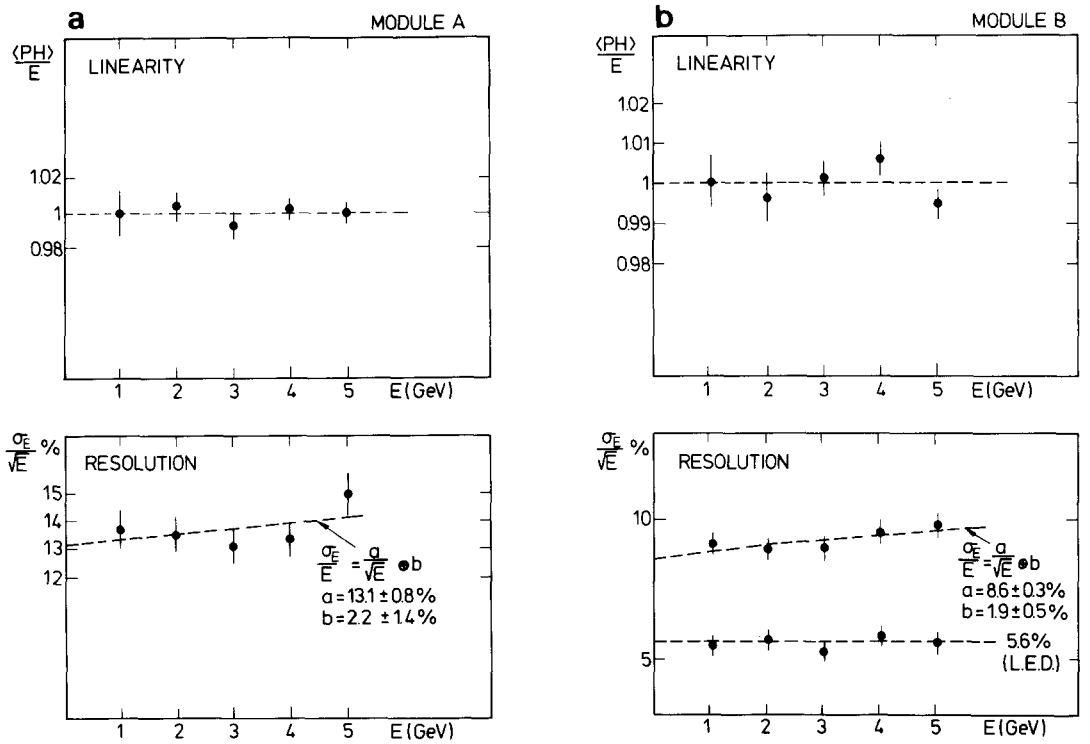

Fig. 3. (a) Linearity and resolution at the center of module A. (b) Linearity and resolution at the center of module B.

The contribution from sampling fluctuations to the resolution can be estimated using the shower Monte Carlo simulation program EGS [8]. In this program, the secondary electrons and photons are followed until they reach some minimum energies, normally 1.5 and 0.1 MeV respectively, and then all their energy is deposited. It turns out that the resolution and average energy deposited in the scintillator depends on these cuts (see fig. 10a). We have used for these quantities the values which follow from extrapolating the cutoff energies to zero: $\sigma = 5.6\%\sqrt{E}$ and 18.9% of the incident electron energy deposited in the scintillator. They also correspond to a semi-infinite medium, but the Monte Carlo also predicts for our finite size calorimeter an energy leakage of 3.2%, mainly transverse and independent of the incident electron energy, and a fluctuation for this leakage of $1.3\%\sqrt{E}$ (see fig. 10b). The resolution of the calorimeter is therefore the quadratic sum of the sampling and the leakage fluctuation:

$$\sigma_{\text{egs}} = 5.8\%\sqrt{E} \quad (E \text{ in GeV}).$$

If we subtract quadratically the contribution of photoelectron statistics from the $\sqrt{E}$ dependent part of the measured resolution, we obtain a resolution (σ_{other} in table 1) of $(9.5 \pm 1.5)\%\sqrt{E}$ for module A and $(6.5 \pm 0.5)\%\sqrt{E}$ for module B. The value for module B is compatible with the resolution predicted by EGS; for module A, however, an additional contribution is not excluded.

The number of photoelectrons per MeV of deposited energy in the scintillator can be calculated from the formula $\sigma_{\text{ph}}/E = 1/\sqrt{N_{\text{ph}}}$ and from the result given by EGS that the fraction of deposited energy in the scintillator is 18.3% once leakage is included. We obtain in this way 0.7 ± 0.2 photoelectrons for module A and 1.7 ± 0.2 for module B. We note that the thickness of the scintillator plates is such that a minimum ionizing particle deposits 0.9 MeV per plate at normal incidence and therefore produces 1.5 photoelectrons.

4. Uniformity of the calorimeter response

Module B was scanned with an electron beam of 3 GeV along three horizontal lines between rows of fibers. The results are shown in fig. 4. The calorimeter is found to be uniform in response within $\pm 1\%$, except in the proximity of a border where energy leakage becomes an important effect. In particular scans along the two symmetric lines shown in fig. 4 give the same result within statistical errors.

We have also measured the calorimeter response when scanning across two neighbouring fibers in the center of the module. The results are shown in figs. 5a

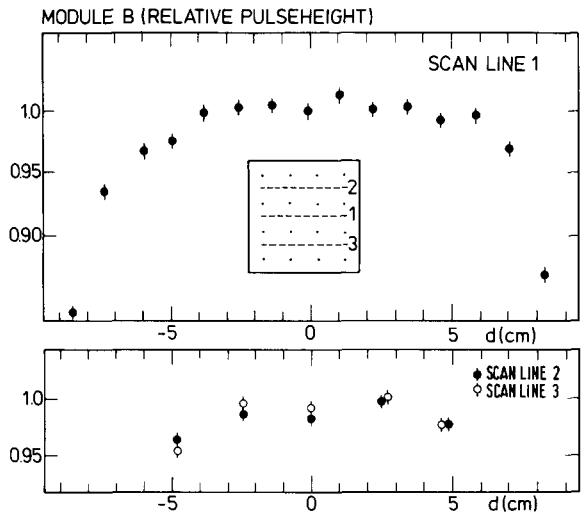

Fig. 4. Result of a scan between rows of fibers for module B. The normalisation is taken at the center of the module.

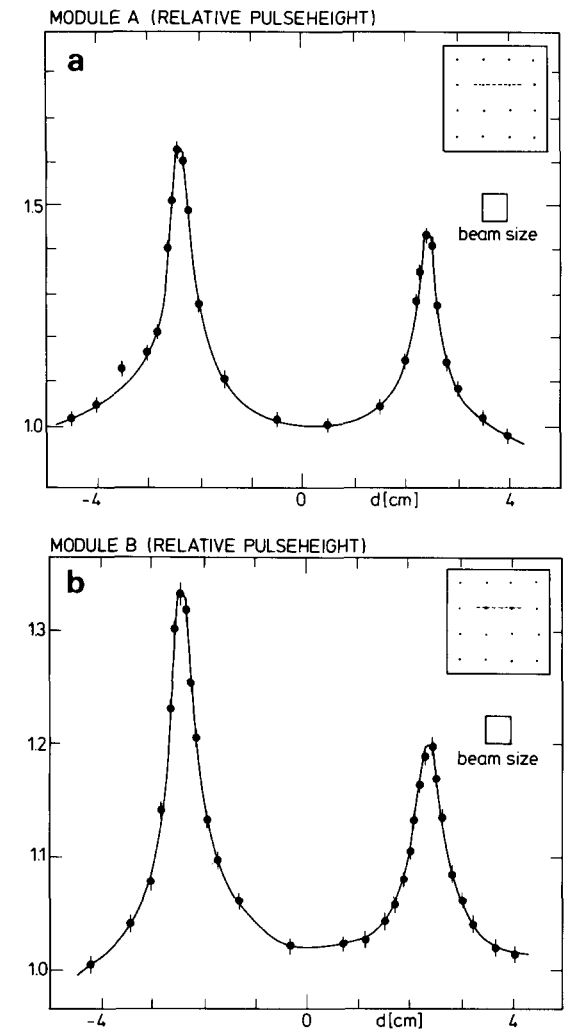

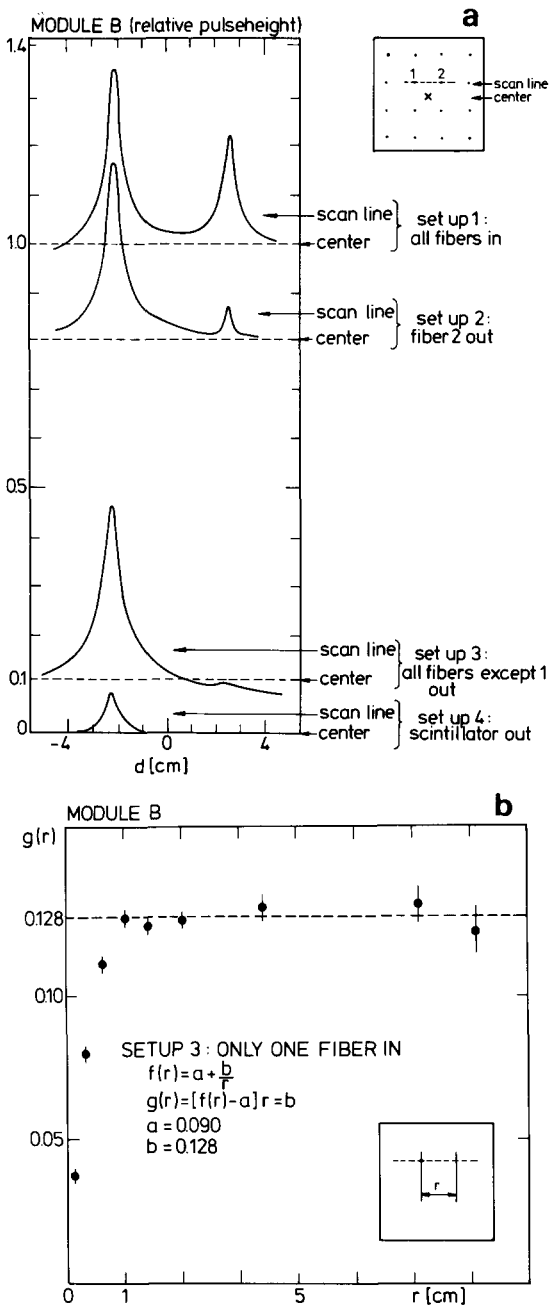

Fig. 6. (a) Investigation of the origin of nonuniformities. Several setups where one or more fibers are missing are considered. The normalisation is taken at the center of the module when all fibers are in place. (b) Verification of the $1/r$ behaviour of the response close to a fiber. The data correspond to the setup 3 of fig. 6a.

Fig. 5. (a) Result of a scan across two neighbouring fibers for module A. The normalisation is taken at the center of the module. (b) Result of a scan across two neighbouring fibers for module B. The normalisation is taken at the center of the module.

and b. One can see that the response at the fiber positions is bigger than at the center of the calorimeter. The enhancement is of the order of 50% for the module equipped with the KSTI-390 scintillator and 20% for the one equipped with SCSN-38. All the pulse height distributions have been normalised to 1 at the centre of the module. Differences at the level of 10% between fibers are also observed.

To investigate the origin of the nonuniform calorimeter response near the fibers we performed scans across fiber positions under various conditions using module B. Fig. 6a shows the measured response for the following setups:

1) module equipped with all 16 fibers (same as fig. 5b),
2) one fiber is pulled out,
3) all fibers but one are pulled out,
4) the scintillator plates are removed and only the fiber stays in the calorimeter.

By comparing the results of (1)–(3) one finds that the response at the fiber position has the same shape independent of the number of fibers in the calorimeter. It is very well described by a $1/r$ dependence, plus a constant term, r being the distance between the impact point and the fiber position. In fig. 6b, which displays the data of setup (3), it is shown that this dependence persists to large distances. At small distances, less than 1 cm, the shower spread and the beam size produce a smearing of this $1/r$ behaviour. In setup (4) the contribution of shower particles creating scintillation and Cherenkov light in the polystyrene fiber is determined. This contribution to the total signal is found to be small. We note also that a small signal enhancement persists at a fiber position even when the fiber has been pulled out. A possible explanation for this effect is that the collected light, coming from late showering inside the hole, suffers less attenuation than in the case of normal showers.

5. Effect of the nonuniformities in the resolution

The energy resolution of the calorimeter depends on the impact position of the beam. We have analysed this dependence for module B. At the center of the calorimeter the resolution has a $\sqrt{E}$ dependence plus a small constant term possibly due to a beam effect. At the fiber position, not only the average pulse height is bigger than at the center but also the distribution is broader and exhibits a tail to higher values. This is shown in figs. 9a and b. If we try again the fit (see fig. 7):

$$\frac{\sigma}{E} = \frac{a}{\sqrt{E}} \oplus b,$$

we find $a = 10.3\%$ and $b = 5.3\%$. The constant term is now significantly bigger than a possible momentum spread from the beam.

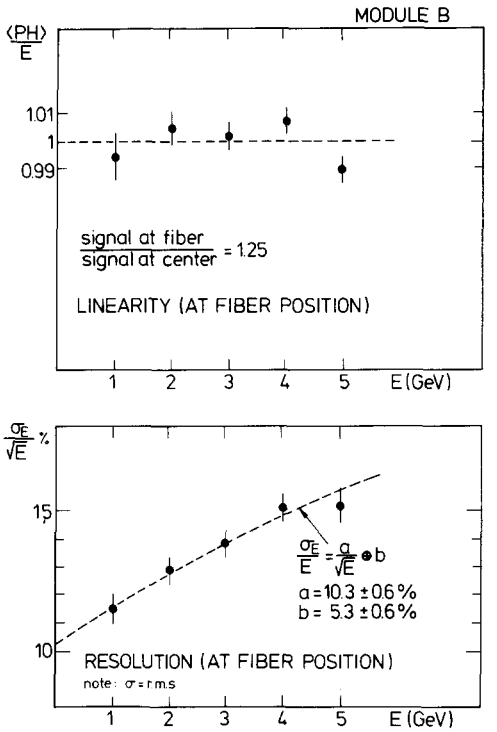

Fig. 7. Linearity and resolution at a fiber position for module B.

A larger calorimeter built in the same way as our test module can be regarded as being composed of successive reflections of one quadrant of the square formed by the innermost 4 fibers as shown in fig. 8a. This is certainly an idealisation since different fiber qualities, cracks between modules and other effects also contribute to the nonuniformities in a real calorimeter. In order to determine the average resolution of such a calorimeter we have performed a scan across the regions 1, 2, 3 and 4 indicated in fig. 8a with the 3 GeV electron beam. Any of these regions is representative of the response of the whole calorimeter and differences can only be attributed to the quality of the fibers themselves. This scan proceeded in steps of 5 mm as indicated in fig. 8b. The result for the scanned regions and the corresponding fibers are summarized in fig. 8c. We see in the case of fiber 1, for example, that there is a 25% increase in the signal at the fiber position with respect to the center of the caolorimeter, whereas this increase is only 3% averaged over the corresponding scanned region. Fig. 9c shows the pulse height distribution averaged over the indicated area in fig. 8a. In fig. 8d we show the resolution at an energy of 3 GeV after subtracting the resolution at the center which is 5.4% at this energy. If we assume again an energy dependence for the resolution of the type $\sigma/E = a/\sqrt{E} \oplus b$, as suggested by the measurements described previously, and take for a the same

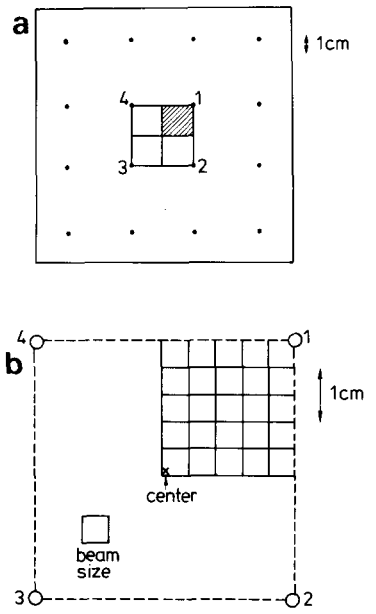

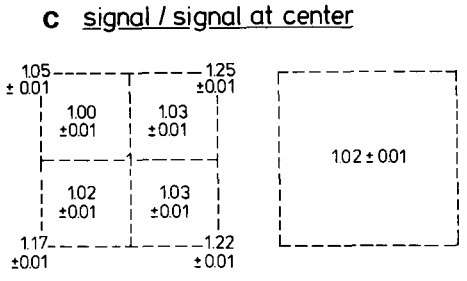

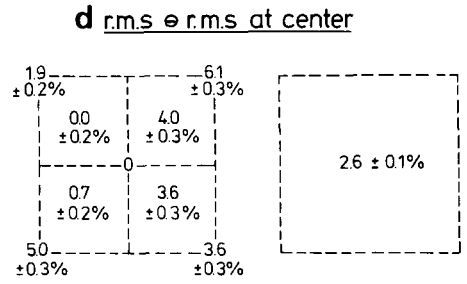

Fig. 8. (a) Position of the four scanned regions inside the calorimeter. Any of them is representative of the whole calorimeter response. (b) A detail of the scan for region 1. This scan proceeds in 25 steps. (c) Response of the calorimeter in the four scanned regions and on average. The signal is normalised to the value at the center of the calorimeter. (d) Resolution of the calorimeter in the four scanned regions and on average. The quoted values result after subtracting quadratically the resolution at the center of the module (⊖ means a quadratic subtraction).

value as in the center, this subtraction procedure gives directly the constant b. We find for example in region 1 a constant term of $b = 4\%$ in addition to the beam effect which is also present at the center.

We note that a bad quality fiber can create around it a more uniform region than the average and then produces a smaller constant b; this is the case for fiber 4 and the reason why the constant b for the average of all 4 regions is only 2.6%.

We can conclude from these measurements that the resolution of the module B if the impact position is not known can be parametrized by:

$$\frac{\sigma}{E} = \frac{a}{\sqrt{E}} \oplus b,$$

where $a \approx 10\%$ and $b \approx 4\%$ in the case where all fibers give a 25% increase with respect to the center of the calorimeter. It should be noted that the energy distribution is not a Gaussian but shows a tail due to the nonuniformities. In case of non-Gaussian distributions we have systematically taken the rms as resolution

6. Monte Carlo simulation

In order to explain our experimental results we have performed a Monte Carlo simulation. This simulation uses the EGS code for shower development and a simulation for the light collection by the fibers (see ref. [9] for more details). The result of this Monte Carlo simulation is a probability for light collected by a single fiber of the type:

$$p(r) = a + \frac{b}{r} e^{-r/\lambda_s} \quad (r > r_0),$$

where r is the distance between the fiber and the point where light is produced, r_0 is the hole radius and λ_s is an effective attenuation length of light inside the scintillator ($\lambda_s \approx 80$ cm for SCSN-38). The parameter a can be interpreted as the contribution of light reaching the fiber after one or more reflections at a lateral surface of the plate, whereas the b term is the contribution of light reeaching the fiber directly. The parameter b depends only on geometrical quantities like the hole radius r_0; for $r_0 = 1$ mm we obtain $b = 1.17\%$ (r in cm). However, a depends both on the reflectivity R at the surface of the plate and on λ_s; this dependence is shown in fig. 11. The $1/r$ behaviour of light collection by a single fiber is in agreement with our data (see figs. 6a and b). The Monte Carlo simulation can in fact reproduce the data of fig. 6a with $a = 0.6\%$ and assuming a uniform beam spot of 4×4 mm^2 (see fig. 12a). It includes also the contribution from particles hitting the fibers. This contribution was tuned in order to reproduce the data of setup 4 in fig. 6a.

When we go to the 16-fiber case, the parametrisation

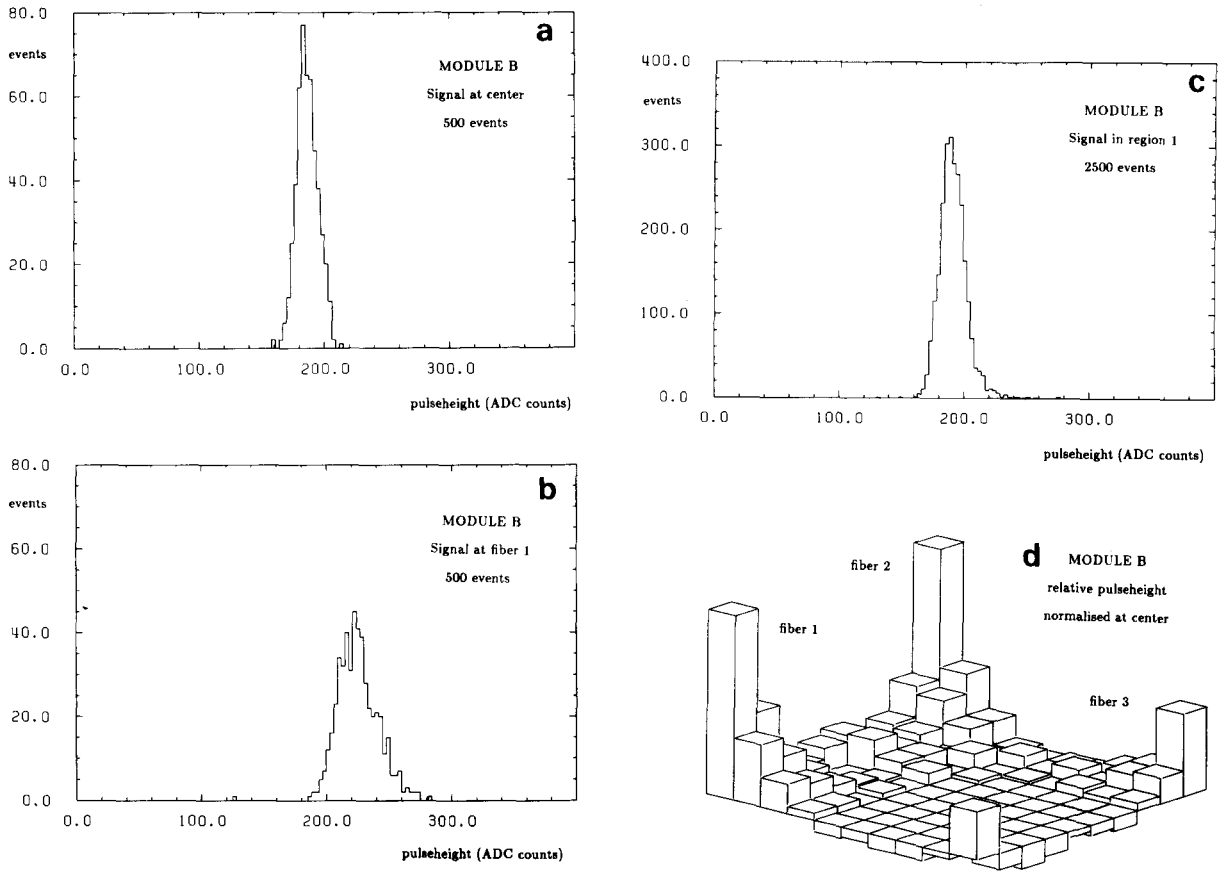

Fig. 9. (a) Pulse height distribution at the center of module B. (b) Pulse height distribution at the position of fiber 1 in module B. Note the tail to high values. (c) Pulse height distribution for the scanned region 1 in module B. Note again the tail to high values. (d) Response of the calorimeter in the four scanned regions. This figure gives a detail of the pulse height for each step of the scan.

for the light probability is:

$$p = p_0 f(p_0),$$

with

$$p_0 = \sum_{i=1}^{16} w_i \left(a + \frac{b}{r_i} e^{-r_i/\lambda_s} \right).$$

f is a function which can be found in ref. [9] and accounts for the screening between fibers; a and b are the same as in the one-fiber case, and r_i is the distance to hole i. Each fiber has a weight w_i; for practical purposes we will take $w_i = 1$ for all fibers. As a consequence each fiber will get a different a parameter. The module B data (see fig. 5b) can be reproduced with the same parameters as for the one-fiber case by simply tuning the a parameter (see fig. 12b). The left fiber response is reproduced with $a = 0.30\%$ and the right fiber with $a = 0.57\%$. These results suggest big differences in the response of individual fibers.

We can calculate as a function of a the response at a fiber position P_f, at the center of the calorimeter P_c, and for the average P_a, with the associated resolutions σ_f, σ_c and σ_a. These quantities are plotted in fig. 13. The resolutions are the constant terms obtained after fit, in the same way as for the data. The Monte Carlo prediction for $a = 0.5\%$ is $P_f/P_c = 1.22$, $P_a/P_c = 1.02$, $\sigma_f/P_f = 5.5\%$ and $\sigma_a/P_a = 2.5\%$. All these values are in agreement with our data. We can also observe that the constant term in the resolution for the average signal, σ_a/P_a, falls below 1% only for very high values of a. We also note that smaller values of λ_s mean also smaller values of a and therefore higher values of P_f/P_c; this explains why module A is less uniform than module B since λ_s is smaller for KSTI-390 than for SCSN-38.

It is also possible to include in the Monte Carlo simulation the attenuation length λ_f along the fibers. We introduce in this way a new constant term in the resolution and deviation from linearity. These deviations, after a linear fit in the range between 1 and 5 GeV, are smaller than 2% even for values of λ_f as small as 40 cm (see fig. 14a). In fig. 14b the dependence of the constant term as a function of λ_f is shown. Our data

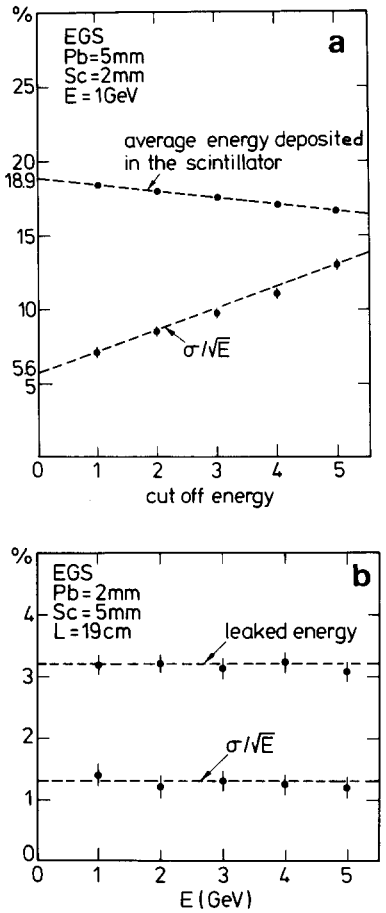

Fig. 10. (a) Energy resolution and average energy deposited in the scintillator, given by EGS for 1 GeV electron showers as a function of the cutoff energies of photons and electrons. These cutoff energies are in units of the minimum values: 1.5 MeV for electrons and positrons and 0.1 MeV for photons. (b) Average value and fluctuation of the leaked energy given by EGS as a function of the incident electron energy.

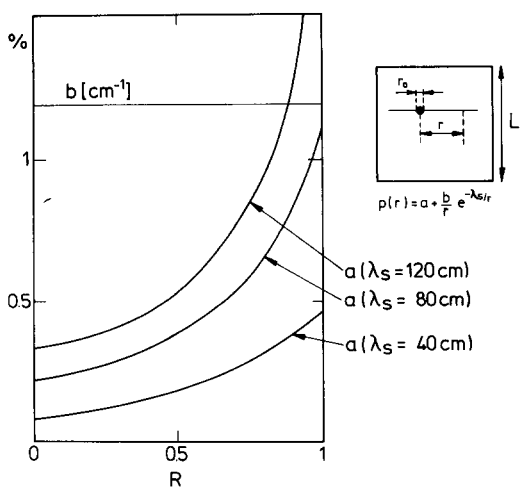

Fig. 11. Dependence of the a parameter on the reflectivity at the surface of the plate R and on the attenuation length of light in the scintillator λ_s.

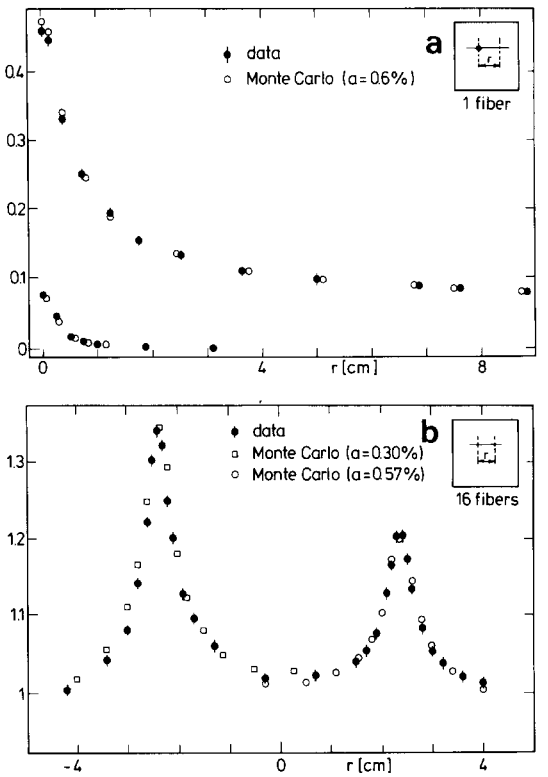

Fig. 12. (a) Comparison between the data and the Monte Carlo prediction for the 1-fiber calorimeter. The data correspond to setups, 3 and 4 in fig. 6a. (b) Comparison between the data and the Monte Carlo prediction for the 16-fiber calorimeter. The data correspond to setup 1 in fig. 6a.

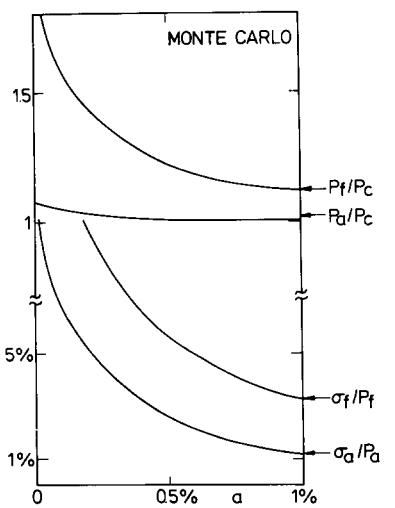

Fig. 13. Monte Carlo prediction for the signal at center, at a fiber position and on average (P_c, P_f, P_a) and the corresponding constant terms in the resolution (σ_c, σ_f, σ_a) as a function of the a parameter.

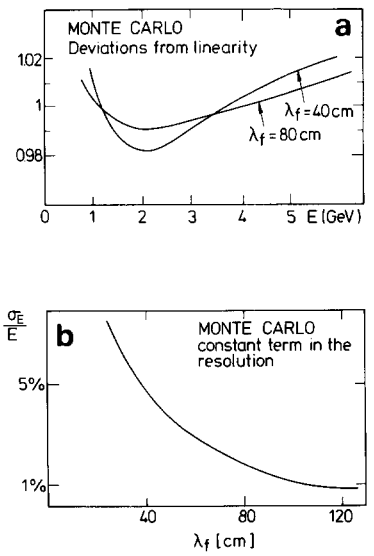

Fig. 14. (a) Monte Carlo prediction for the deviations from linearity due to the attenuation length λ_f along the fibers. (b) Monte Carlo prediction for the constant term in the resolution due to the attenuation length λ_f along the fibers.

for module B are compatible with a value of λ_f greater than 60 cm; if λ_f is greater than 1 m, the constant term falls down below 1%.

7. Conclusions

We have tested an electromagnetic calorimeter of the lead–scintillator sandwich type with fiber readout. We have considered two scintillator options: KSTI-390 and SCSN-38. We used for both options 16 polystyrene fibers doped with K27 in a concentration of 400 mg/l.

The best resolution is achieved with the calorimeter equipped with SCSN-38 scintillator. This resolution is $\sigma = 8.6\%\sqrt{E}$ at the center of the calorimeter, corresponding to $5.8\%\sqrt{E}$ from sampling fluctuations and $5.6\%\sqrt{E}$ from photostatistics. This combination satisfies the requirement of providing enough light (about 1.5 photoelectrons per minimum ionising particle and plate).

However, the presence of fibers leads to nonuniformities in the response of calorimeter from a geometrical origin (the response varies like $1/r$ plus a constant, where r is the distance to the fiber). If the impact position at the calorimeter surface is not known, these nonuniformities translate into a constant term in the expression of σ/E which is of the order of 4% for the test module considered. This constant term will dominate the resolution for electrons above 6 GeV. Additional contributions to this constant term due to boundaries or a nonuniform fiber density are also expected in a calorimeter as proposed in the ZEUS letter of intent [2].

Acknowledgements

We gratefully acknowledge K. Westphal for taking care of the mechanical construction of the modules. We are very grateful for fiber material obtained from Saclay, France and Kyowa-Gas, Japan. We would like also to thank E. Hilger, R. Klanner, H. Kowalski, L. Labarga, G. Levman and G. Wolf for helpful discussions. This study was supported by the Bundesministerium für Forschung und Technologie, Germany and CAICYT, Spain. One of us (F.B.) would like to thank Prof. Brandt for his hospitality at Siegen University and the Deutsche Forschungsgemeinschaft for financial support.

References

[1] Experimentation at Hera, DESY HERA 83/20 (October 1983).
[2] ZEUS letter of intent, DESY (June 1985).
[3] H. Fessler et al., Nucl. Instr. and Meth. A240 (1985) 284.
[4] Produced by J.C. Thevenin et al. at CEN-Saclay.
[5] Experimental product of Hoechst, Germany.
[6] Product of KSH, Belgium.
[7] Product of Kyowa-Gas, Japan.
[8] R.L. Ford and W.R. Nelson, SLAC Report 210 (1978); the version used is EGS3.
[9] L. Labarga and E. Ros, Siegen University preprint SI-86-07.